



**HAL**  
open science

# Elastohydrodynamic Film Formation and Sol/Gel Transition of Aqueous Fluids

Keiji Asada, Juliette Cayer-Barrioz, Denis Mazuyer

► **To cite this version:**

Keiji Asada, Juliette Cayer-Barrioz, Denis Mazuyer. Elastohydrodynamic Film Formation and Sol/Gel Transition of Aqueous Fluids. Tribology Letters, 2022, 70 (4), pp.97. 10.1007/s11249-022-01640-0 . hal-03765872

**HAL Id: hal-03765872**

**<https://hal.science/hal-03765872v1>**

Submitted on 28 Oct 2022

**HAL** is a multi-disciplinary open access archive for the deposit and dissemination of scientific research documents, whether they are published or not. The documents may come from teaching and research institutions in France or abroad, or from public or private research centers.

L'archive ouverte pluridisciplinaire **HAL**, est destinée au dépôt et à la diffusion de documents scientifiques de niveau recherche, publiés ou non, émanant des établissements d'enseignement et de recherche français ou étrangers, des laboratoires publics ou privés.



# Elastohydrodynamic Film Formation and Sol/Gel Transition of Aqueous Fluids

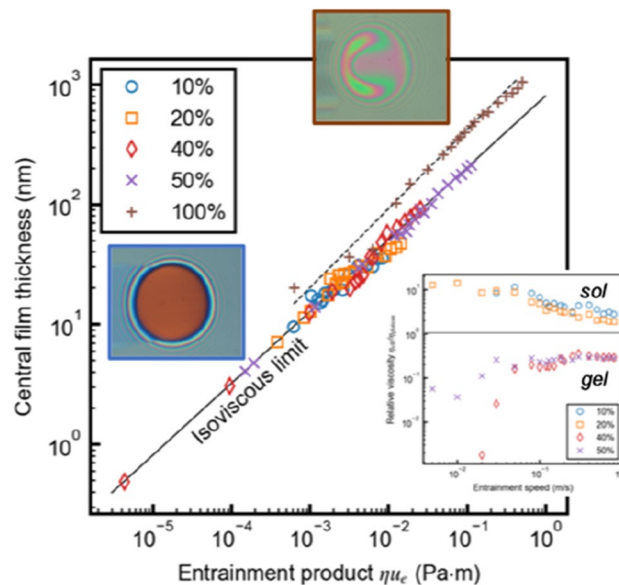
K. Asada<sup>1,2</sup> · J. Cayer-Barrioz<sup>2</sup> · D. Mazuyer<sup>2</sup>

Received: 27 April 2022 / Accepted: 28 July 2022  
© The Author(s) 2022

## Abstract

One of the most widely used water soluble lubricants is PolyAlkylene Glycol (PAG). PAG aqueous solutions can form a gel depending on the concentration and temperature, which affects the formation and friction of lubricating films. This experimental work combined rheological measurements and in-situ film-forming analysis in pure rolling conditions using PAG aqueous solutions of various concentrations. It shows that the pure PAG behaved classically as a piezoviscous fluid, while its aqueous solutions behaved as isoviscous fluids. This was confirmed by the establishment of a film formation map. In addition, the aqueous solutions exhibited two behaviors, characteristic of either sol or gel. A detailed analysis of the film thickness evolution, based on Moes–Venner’s predictions, allowed us to calculate the effective viscosity in the inlet zone and to discuss the origin of the two families, sol vs gel.

## Graphical Abstract



**Keywords** Aqueous lubrication · EHL · Film formation · Sol/gel transition

✉ J. Cayer-Barrioz  
juliette.cayer-barrioz@ec-lyon.fr

<sup>1</sup> Lubricants Research Laboratory, Idemitsu Kosan Co. Ltd.,  
24-4 Anesakikaigan, Ichihara, Chiba 299-0107, Japan

<sup>2</sup> Laboratoire de Tribologie et Dynamique des Systèmes,  
CNRS UMR 5513, Ecole Centrale de Lyon, 36 avenue Guy  
de Collongue, 69134 Ecully Cedex, France

## Abbreviations

$c_{\text{eff}}$  Effective concentration (%)  
 $E_{b,d}$  Young’s modulus (respectively, ball and disk)  
(Pa)  
 $E'$  Reduced Young’s modulus (Pa),  
$$E' = \frac{2}{\{(1-\nu_b^2)/E_b + (1-\nu_d^2)/E_d\}}$$

EHL	Elastohydrodynamic lubrication
EO	Ethylene oxide
$G$	Dimensionless material parameter (Hamrock & Dowson), $G = \alpha E'$
$h_c$	Central film thickness (m)
$H_{cen}$	Dimensionless central film thickness, $H_{cen} = \frac{h_c}{R_x U}$
$H_{RI}$	Dimensionless central film thickness for the rigid-isoviscous condition
$H_{RP}$	Dimensionless central film thickness for the rigid-piezoviscous condition
$H_{EI}$	Dimensionless central film thickness for the elastic-isoviscous condition
$H_{EP}$	Dimensionless central film thickness for the elastic-piezoviscous condition
$K$	Thermal conductivity (W/(m·K))
$L$	Dimensionless lubricant parameter (Moes), $L = G(2U)^{0.25}$
$M$	Dimensionless load parameter (Moes) for point contact, $M = \frac{W}{(2U)^{0.75}}$
PAG	Polyalkylene glycol
PEG	Polyethylene glycol
PO	Propylene oxide
$R_x$	Reduced radius of curvature parallel to the entrainment direction (m)
$R_y$	Reduced radius of curvature perpendicular to the entrainment direction (m)
$s$	Parameter in Moes–Venner's equation
$T_{gel}$	Gelation temperature ( °C)
$T_{inlet}$	Inlet temperature ( °C)
$u_e$	Mean entrainment speed (m/s)
$u_s$	Sliding speed (m/s)
$U$	Dimensionless speed parameter (Hamrock & Dowson), $U = \frac{\eta u_e}{E' R_x}$
$w$	Normal load (N)
$W$	Dimensionless load parameter (Hamrock & Dowson), $W = \frac{w}{(E' R_x^2)}$
$\alpha$	Pressure-viscosity coefficient (Pa <sup>-1</sup> )
$\eta$	Viscosity of fluid
$\eta_{eff}$	Effective viscosity
$\eta_{plateau}$	Viscosity at a shear rate of 10 <sup>3</sup> s <sup>-1</sup> (second Newtonian plateau)
$\lambda$	Gap curvature ratio, $\lambda = \frac{R_x}{R_y}$
$\nu_{b,d}$	Poisson's ratio (respectively, ball and disk)

## 1 Introduction

ElastoHydrodynamic Lubrication (EHL) describes a lubrication regime in which a full film well separates two elastically deformed surfaces in contact. In high-pressure contacts,

the formation of this separating film usually results from the combination of four main effects: the formation of a hydrodynamic film, the contact geometry, the solid elastic deformation, and the increase in fluid viscosity with pressure. Film thickness predictions successively developed by Ertel [1], Hamrock and Dowson [2], and Moes and Venner [3] were based on certain hypotheses, such as a continuous and homogeneous medium, fully flooded contact, and piezoviscous fluids in the case of Hamrock and Dowson [2]. Moes–Venner's predictions remain valid over a wider range of conditions and include asymptotic solutions for isoviscous fluids [3], [4].

Despite being isoviscous, in the presence of numerous additives, water meets all the requirements in terms of heat transfer and lubricity, to be the perfect lubricant candidate for food and cosmetics as well as wire-drawing processes.

Among the aqueous supramolecular solutions used as lubricants, polymer and lamellar solutions have been extensively investigated at the molecular scale in the boundary lubrication regime regarding their friction mechanisms [5], [6], [7], [8]. In EHL conditions, two contributions govern the film-forming mechanisms of these solutions: the formation of an adsorbed boundary film on the surfaces and a hydrodynamic contribution [4], [9], [10]. In the case of heterogeneous media such as water/oil emulsions, the bulk properties are similar to those of water at low oil concentration, meaning that low viscosity is combined with the absence of piezoviscosity. Film build-up mechanisms are then complex, depending on the emulsifier, its concentration, and the oil concentration [4], [11], [12]. The evolution of film thickness vs. entrainment velocity is well described in the literature [13]. Three regimes have been distinguished: at low velocities, a first regime in which the film thickness increases with the velocity; a second regime, at intermediate velocities, in which the film thickness suddenly decreases with an increasing velocity, and in the third regime, it starts growing again at high velocities. A few mechanisms were identified and discussed in [13], [14], [15], [16], [17], [18]. The formation, in the contact inlet, of an oil reservoir supplying the contact at low velocities could explain the first regime in which the film thickness establishment is then governed by the bulk oil properties. The following regimes could result from an inversion of phase in the reservoir, richer in water than in oil, meaning that the contact would be starved in oil. The higher the oil concentration, the thicker the film. However, no consensus was reached on the influence of the size of the oil droplets. The affinity of the emulsifier with the surface could also contribute to the formation of an oil-rich reservoir.

Most of the recent works on gel lubrication focus on rubbing two hydrogels against each other (see [19])

for instance). The friction mechanisms involve surface structure and water network interactions as well as bulk behavior such as gel elasticity and flow. The question of gel film-forming mechanisms in a contact remains unaddressed.

However, a rather simple molecule, PolyAlkylene Glycol (PAG), composed of Ethylene Oxide (EO) and/or Propylene Oxide (PO) units, can be used to control the sol/gel transition of aqueous solutions. PAG is a synthetic base stock used in various kinds of lubricants, such as gear oil, hydraulic fluid, rolling oil, cutting fluid, and grinding fluid. Compared to mineral oil and other synthetic lubricants, PAG has some advantages, such as a high viscosity index, low pour point, high flash point, and a wide range of solubility [20]. These features derive from the molecular structure of PAG, whose properties can be controlled by changing the molecular weight, the EO weight fraction, and block structures. Notably, the higher EO/PO ratio enables PAG molecules to dissolve in water [21].

Under EHL conditions, the concentration of PAG in water significantly affects the film-forming capability. Zhang et al. [22] reported that the film-forming characteristics of PAG aqueous solutions with concentrations larger than 50% could be described by Hamrock–Dowson's equation [2] similarly to the case of piezoviscous oil lubricants. Nevertheless, this prediction was not followed for concentrations lower than 50%. Zhang et al. [22] also mentioned that the pressure–viscosity coefficient of PAG solutions decreases with a concentration diminution. In addition, they showed that the larger molecular weight of PAG contributed to the formation of a thicker lubricating film. This result was attributed to the high viscosity of the aqueous solution with larger molecular weight PAG. Shuhai et al. [23] suggested a lubrication map of linear polymer in aqueous solution. It is defined by the ratio of the water film thickness to the average radius of polymer chains  $H/R_{\text{polymer}}$  using various molecular weights of PolyEthylene Glycol (PEG): the film thickness of PEG aqueous solutions decreased as the polymer molecular weight increased when  $\frac{H}{R_{\text{polymer}}} < 2 - 3$  [23].

This brief literature review shows that the film-forming capability of aqueous solutions and gels is not yet fully understood. In this context, this work aims at understanding the film-forming mechanisms of aqueous solutions and gels in EHL conditions. To address this problem, a combined rheological and film-forming characterization was experimentally performed using aqueous solutions of various concentration of PAG. It is shown that their flow dynamics is a thermally activated phenomenon. Finally, the evolution of film thickness was analyzed and discussed in terms of piezo- vs iso-viscosity, effective viscosity, and effective concentration of the lubricant inside the contact convergent.

## 2 Experimental Details

### 2.1 Lubricants

PAG used in this study was ADEKA Pluronic L-64, provided by ADEKA Corporation, which is triblock copolymer composed of two EO blocks sandwiching a PO block. The molecular weight and the weight fraction of EO blocks were equal to  $2900 \text{ g mol}^{-1}$  and 40%, respectively. Aqueous solutions were prepared by diluting the PAG molecules with deionized water at concentrations ranging from 10 to 50%. Pure PAG (100%) was also investigated.

The rheological properties of the pure PAG and its aqueous mixtures were investigated using MCR302 (Anton Paar GmbH) with a cone-plane geometry. The cone diameter was 74.983 mm and the cone angle was  $1.005^\circ$ , respectively. Two protocols were performed to measure the viscosity, as summarized in Table 1: the first one consisted in varying the shear rate from  $10^{-2}$  to  $10^3 \text{ s}^{-1}$  at a fixed temperature, here  $22^\circ\text{C}$ ; the second one consisted in varying the temperature from 0 to  $60^\circ\text{C}$  for the PAG aqueous solutions (conversely, from 60 to  $0^\circ\text{C}$  for the pure PAG, as its melting point was around  $15^\circ\text{C}$ ) at a fixed shear rate of  $10^3 \text{ s}^{-1}$ .

### 2.2 Film Thickness Measurements

Film thickness measurements were performed using the IRIS tribometer, detailed in the literature in [24]. This apparatus creates an EHL point contact between a ball and a transparent disk under controlled contact kinematics, while simultaneously measuring the contact forces and visualizing the film thickness distribution. The ball was here made of AISI 52,100 steel with a diameter of 19.05 mm, and. The 60 mm-diameter disk was made of silica with two coating layers: a 6 nm-thick semi-reflective chromium layer and a 200 nm-thick silica spacer layer on top of the chromium layer. Two independent brushless motors independently and accurately controlled the velocity of the ball velocity and the disk, ranging from  $0.005 \pm 0.001$  to  $0.8 \pm 0.01 \text{ m/s}$ . Experiments were carried out under pure rolling conditions with an applied load of  $15 \pm 0.5 \text{ N}$ , corresponding to a mean contact pressure of 305 MPa and Hertzian contact radius of  $125 \mu\text{m}$ , at ambient temperature ( $20 \pm 3^\circ\text{C}$ ). The detailed experimental protocol, including surface preparation, i.e., polishing, cleaning, and roughness characterization, can be

**Table 1** Protocols of rheological measurements

Protocol	Shear rate ( $\text{s}^{-1}$ )	Temperature ( $^\circ\text{C}$ )
Shear varying	$10^{-2}$ – $10^3$	22
Temperature varying	$10^3$	0–60 or reverse

found in [24]. The film thickness was obtained using the interferometry technique with the appropriate calibration, taking the refractive index of the fluid into account.

### 3 Results

#### 3.1 Viscosity Measurement

Figure. 1 shows the dynamic viscosity plotted versus shear rate at a temperature of 22 °C for the PAG aqueous solutions with concentrations of 10 to 50%. In this range of PAG concentrations, the viscosity increased as PAG content increased. Additionally, the solutions exhibited shear-thinning behavior at a shear rate ranging from  $10^{-2}$  to  $10^1$  s<sup>-1</sup>. It is noteworthy that a much larger magnitude of shear-thinning behavior was observed at a much lower shear rate than that of conventional oil-type lubricants. The viscosity reached a second Newtonian plateau above a shear rate of  $10^2$  s<sup>-1</sup>. In this work, the viscosity of the second Newtonian plateau  $\eta_{plateau}$  was concretely defined as the viscosity at a shear rate of  $10^3$  s<sup>-1</sup>. The viscosity values are reported in Table 2. These values were compared to those calculated with Arrhenius mixture law: the large discrepancy seems to indicate that this mixture law cannot describe the physics at stake here in the considered model fluids.

Figure. 2 presents viscosity variations of the PAG aqueous solutions as a function of temperature at a shear rate of  $10^3$  s<sup>-1</sup> when the viscosity reached the second Newtonian

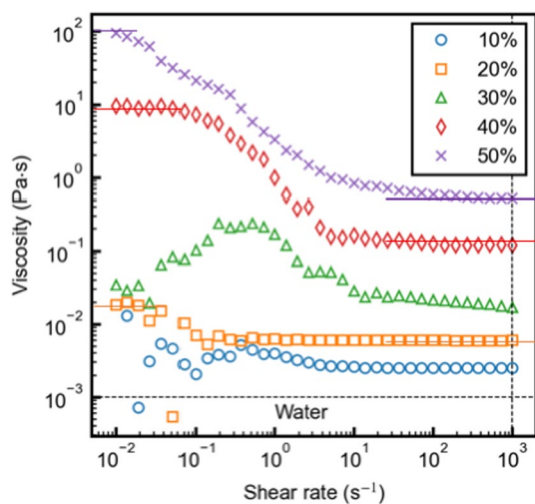


**Fig. 1** Viscosity versus shear rate at a temperature of 22 °C. All PAG aqueous solutions showed shear-thinning at shear rates ranging from  $10^{-2}$  to  $10^1$  s<sup>-1</sup>. Two continuous lines were added to indicate the first and second viscosity plateau. The horizontal dashed line corresponds to the viscosity of water. The vertical dashed line indicates the shear rate at which the viscosity was measured against temperature (values reported in Table 2). At this value of  $10^3$  s<sup>-1</sup>, the viscosity appeared to reach its second Newtonian plateau

**Table 2** Viscosity of second Newtonian plateau  $\eta_{plateau}$  and average effective viscosity at  $u_e > 0.1$  m/s. For the pure PAG, was measured in the temperature varying protocol (superscript \*)

PAG concentra- tion (%)	Viscosity of second Newtonian plateau $\eta_{plateau}$ (Pa·s)	Average effective viscosity at $u_e > 0.1$ m/s (Pa·s)
100	0.624*	–
50	0.525	0.141
40	0.121	0.0319
20	0.00599	0.0178
10	0.00251	0.0104

plateau. The semi-logarithmic plot of the viscosity first showed a linear decrease and subsequently reached a minimum value before rising again. This evolution suggested the occurrence of the gelation process. The latter was then characterized by the value of the temperature at which the mixture viscosity started increasing. It can be noticed that the evolution of the viscosity of the pure PAG with temperature coincides with the upper envelope of viscosity–temperature curves of aqueous PAG solutions for temperatures higher than 10 °C. During this rheological measurement, the 40 and 50% PAG aqueous solutions finally became gels and scattered from the gap of the cone-plane, leading to an apparent drop of the viscosity at high shear rates. Consequently, the viscosity could not be measured over the entire temperature range.

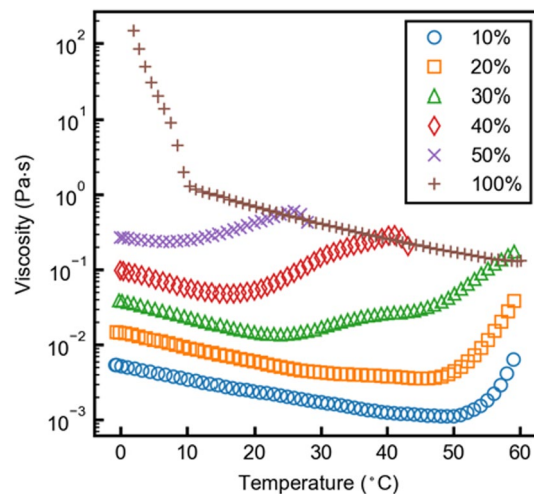


**Fig. 2** Evolution of the viscosity versus temperature at a shear rate of  $10^3$  s<sup>-1</sup>. Each PAG aqueous solution exhibited a minimal value, which was defined as the gelation temperature. Below this gelation temperature, the slope of the viscosity vs the inverse of temperature was interpreted in terms of activation energy

### 3.2 Film-Forming Capability in Pure Rolling

Figure 3 a shows the central film thickness evolution versus the mean entrainment speed for the pure PAG and the four PAG aqueous solutions in pure rolling condition at ambient temperature. For all solutions, the central film thickness increased with the entrainment speed; however, the magnitude of the increase depended on the concentration. The more concentrated, the thicker the film. Figure 3b–f shows contact interferograms at an entrainment speed of 0.5 m/s. The lubricating film was homogeneous in the high-pressure zone and a classical EHL horse-shoe shape was observed, revealing the film constriction.

## 4 Discussion

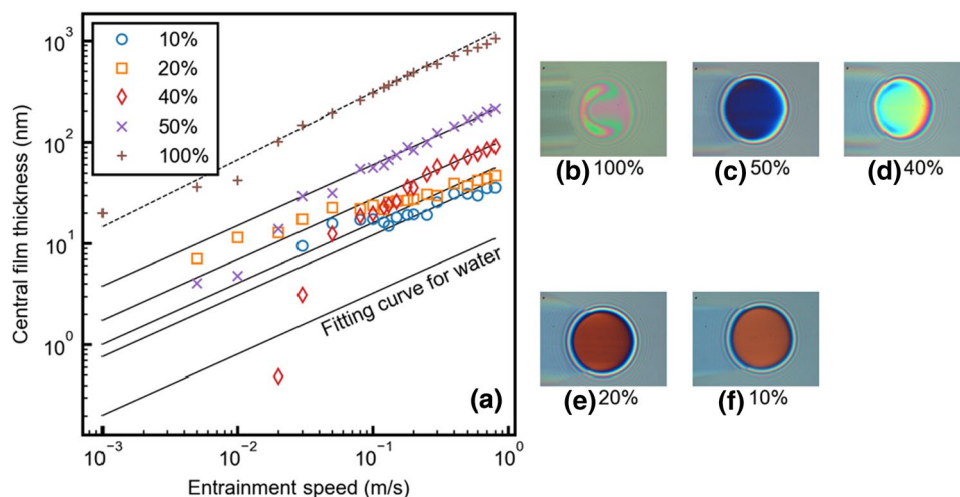
### 4.1 Sol/Gel Transition

According to de Gennes [25], the sol/gel transition can be classically pictured using the “tree” approximation. The origin of the physical branching between the polymeric chains can be assumed here as the intermolecular hydrophobic interactions, resulting in the progressive freezing of a certain number of degrees of freedom. Figure 2 shows the dependence of the extension of the temperature interval of sol/gel transition with the concentration: it is very marked for 10% but wider for the concentrations over 20%. The existence of this crossover region could

be the signature of a weak gelation process in which the crosslinks are not completely stable, resulting from the kinetics of bonding/nonbonding reactions. The more concentrated, the higher number of bonding possibilities/chains and consequently a lower gelation temperature. We consider here a weak physical gel as introduced by de Gennes [25]. The presence of non-covalent crosslinks would explain:

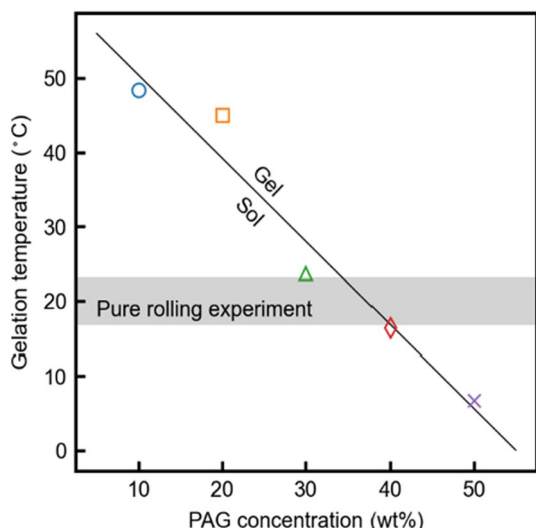
- the change in viscosity with temperature in Fig. 2 (viscosity is proportional to  $1/T$ ),
- the change in appearance of the blend that was observed,
- the very low values of  $G'$ , hardly measurable at 22 °C over 4 decades of frequency for the 10 and 20% concentration blends,
- the fact that significant values of  $G'$  were only measured for concentrations over 40%.

Figure 4 shows the gelation temperature  $T_{gel}$ , which was defined here as the temperature at which the viscosity reached the minimum value on the rheograms shown in Fig. 2.  $T_{gel}$  decreased linearly as the concentration increased. This graph also suggests that the PAG solutions can be expected to behave differently in terms of film-forming capability, as the pure rolling experiments were carried out at ambient temperature (indicated with the grey zone on Fig. 4): the low concentrated solutions at 10 and 20% were in a liquid state, while the more concentrated mix at 40 and 50% was in the gel state a priori. Additionally, this plot indicates that the concentration at which the transition occurs at room temperature is about 35%.



**Fig. 3** a Central film thickness versus entrainment speed in logarithmic scale. The solid line corresponds to Moes–Venner’s prediction: for the pure PAG with a viscosity of 0.624 Pa·s and pressure viscosity coefficient of 11.8  $\text{GPa}^{-1}$ , and for the others with an average effective viscosity (see Table 2) and pressure viscosity coefficient of

0.4  $\text{GPa}^{-1}$ , corresponding to that of water. The prediction curve for water, an isoviscous fluid, was also calculated with Moes–Venner’s equation using a viscosity of 1 mPa·s and plotted; b–f contact interferograms at an entrainment speed of 0.5 m/s. The contact diameter was about 250  $\mu\text{m}$  and the fluid flowed from right to left



**Fig. 4** Gelation temperature of each PAG aqueous solutions. The solid line corresponds to the sol–gel transition. An aqueous solution containing approximately 35% of PAG or more would behave as a gel at the temperature used during pure rolling experiments

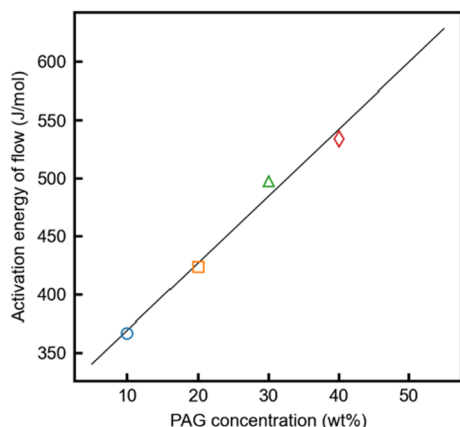


**Fig. 5** Activation energy of the flow versus PAG concentration. The activation energy was calculated from the slope of  $\log(\text{viscosity})$  to inverse of temperature curve below gelation temperature. The solid line corresponds to a linear regression. For the 50% PAG aqueous solution, the activation energy could not be calculated from the data in Fig. 2

### 4.2 The Origin of the Viscous Flow

To analyze the origin of the viscosity evolution, it was assumed that the balance between the thermal mobility and the interactions of molecules determines the activation energy of the flow for the PAG aqueous solutions. Figure 5 shows the activation energy, which was calculated from the slope of the  $\ln\eta - (1/T)$  curve below the gelation temperature, as a function of the PAG concentrations. The activation energy of the flow is proportional to the PAG

concentration ranging from 10 to 40%; that is to say, the viscosity of the sol phase of PAG aqueous solutions arises from the same dominant interactions between molecules, which increase with the PAG concentration. The sol/gel transition is out of the range of the viscosity–temperature measurement for the 50% PAG aqueous solution, which is why it was not reported in Fig. 5.

Above the gelation temperature, the slopes of the  $\ln\eta - (1/T)$  plots were negative: therefore, the viscosity was no longer dominated by the same interactions as those occurring under the gelation temperature. The influence of the viscosity kinetics was further investigated in a lubricated contact.

### 4.3 Film-Forming Capability and Rheological Characteristic

To analyze the film-forming properties of these solutions, Moes–Venner’s formula [3] was used

$$H_{cen} = \left[ \left\{ H_{RI}^{3/2} + (H_{EI}^{-4} + 0.1\lambda^4)^{-3/8} \right\}^{2s/3} + (H_{RP}^{-8} + H_{EP}^{-8})^{-s/8} \right]^{1/s} \tag{1}$$

$$s = \frac{3}{2} \left\{ 1 + e^{(-1.2H_{EI}/H_{RI})} \right\}. \tag{2}$$

For the point contact,  $\lambda = 1$ , then  $H_{cen}$  can be expressed as follows (3):

$$H_{RI} = 41.34M^{-2}$$

$$H_{RP} = 0.9089L^{2/3}$$

$$H_{EI} = 2.419M^{-2/15}$$

$$H_{EP} = 1.247M^{-1/12}L^{3/4}.$$

As presented in the above equations, Moes–Venner’s formula describes the film thickness using the rigid-isoviscous, rigid-piezoviscous, elastic-isoviscous, and elastic-piezoviscous terms to describe the overall film thickness. This enables us to analyze film-forming properties for both piezoviscous and isoviscous fluids.

On the one hand, Fig. 3a shows that the pure PAG film thickness varies with  $u_e^{0.67}$  (see straight dashed line) following the Moes–Venner prediction [3] for a piezoviscous fluid. For the pure PAG, the slight deviation of the measured points to this law suggests the occurrence of starvation in the range of velocities above roughly 0.2 m/s, due to the combination of the high viscosity of pure PAG (0.624 Pa·s) and a high entrainment speed. However, the

slope of the straight line of 0.67 remained reasonable, meaning that the pure PAG should be treated as a piezoviscous liquid.

For the aqueous solutions, on the other hand, the slope of the straight lines in the logarithmic scaling of the thickness vs. velocity curves is 0.60, which is similar to the one obtained for water, as shown in Fig. 3a. This indicates that these aqueous solutions should rather be treated as isoviscous fluids.

In this framework, for the pure PAG, a pressure viscosity coefficient of  $11.8 \text{ GPa}^{-1}$  was then calculated from Eq. (1) using the data obtained for entrainment speed below 0.2 m/s. Assuming that the aqueous solutions were isoviscous (that is to say with a viscosity practically independent of the pressure: here, using a pressure viscosity coefficient equaled that of water of  $0.4 \text{ GPa}^{-1}$ – $0.36$  at  $55 \text{ }^\circ\text{C}$  in [26]), the effective viscosity was then calculated from Eq. (1). Figure 6 shows the relative viscosity, calculated as the ratio of the effective viscosity divided by the plateau viscosity. Two “families” can be distinguished: one corresponding to 50 and 40% and the other to 20 and 10%. It is noteworthy that the relative viscosity was less than unity for the 40 and 50% solutions, corresponding to gel and plug flow in the convergent zone, while it was higher than unity and decreased as the velocity increased for the lower concentrations. This trend is very similar to that observed for emulsions where the higher viscosity at low velocity can account for the presence of oil droplets in the convergent zone and the decrease with the velocity was explained by phase change [15, 17]. In this context, one could assume an analogy between oil droplets and PAG polymer droplets.

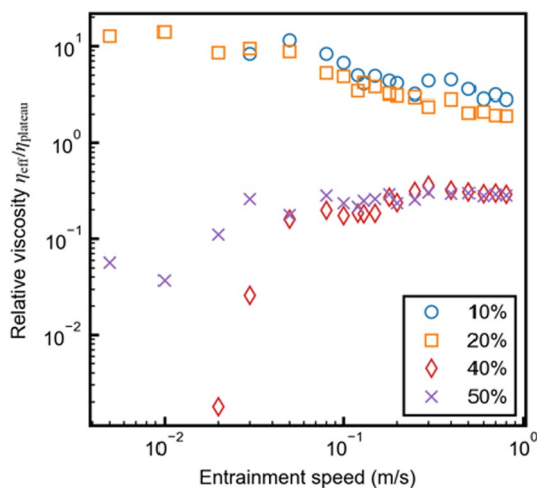


**Fig. 6** Relative viscosity  $\eta_{\text{eff}}/\eta_{\text{plateau}}$  at each entrainment speed for the aqueous solutions. For the low concentration, relative viscosity was larger than unity and decreased as the entrainment speed increased. For the higher concentration, the relative viscosity was less than unity and collapsed below approximately 0.05 m/s

This interpretation and the existence of these two families were also confirmed by the solution appearance as either gel or sol. In addition, during the pure rolling experiments, the ambient temperature was either below or above the gelation temperature.

In the contact inlet, the shear rates reach  $10^6$ – $10^7 \text{ s}^{-1}$ , much higher than the shear rates applied in rheology. Nevertheless, the second viscosity plateau was attained for shear rates lower than  $10^3 \text{ s}^{-1}$  (as shown in Fig. 2). We then assumed that this second viscosity plateau could be considered as an order of magnitude of the viscosity at higher shear rates and used it for comparison with the effective viscosity. If further shear-thinning occurs, the ratio of the effective viscosity divided by the viscosity plateau would increase, getting close to one for 40 and 50%. This ratio would remain higher than one for 10 and 20%.

This discussion can be graphically summarized by plotting a “film formation map” based on the evolution of the central film thickness versus effective entrainment product (effective viscosity  $\times$  entrainment speed), as shown in Fig. 7. The plot for piezoviscous fluids (here the pure PAG) was well described by the straight dashed line with a 0.67 gradient. Conversely, for isoviscous fluids, the data collapsed on one straight line characteristic of the “isoviscous limit”.

#### 4.4 Film-Forming Mechanisms

The film-forming mechanisms of the PAG aqueous solutions can then be further discussed from the viewpoint of the flow conditions at the inlet zone and the surface.

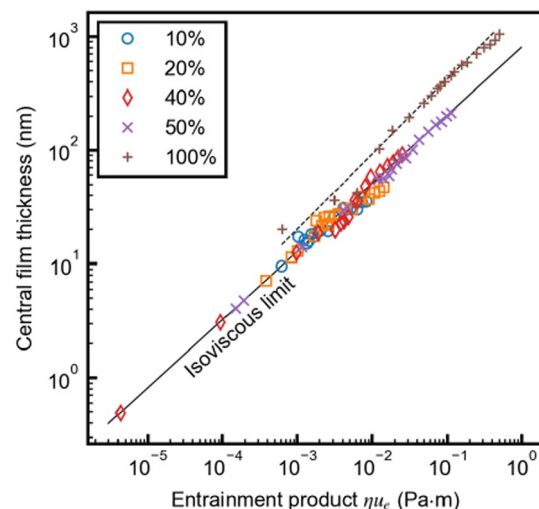


**Fig. 7** Film formation map expressing central film thickness versus entrainment product (viscosity  $\times$  entrainment speed). The dashed line corresponds to Moes–Venner’s prediction for the piezoviscous pure PAG and the solid line corresponds to the isoviscous limit, on which all isoviscous solutions collapsed



First, to consider the sol/gel transition at the inlet zone, the temperature rise due to shear heating is estimated. Guilbault [27] proposed the average temperature increase at the inlet zone under the rolling-sliding condition as follows:

$$\overline{\Delta T}_{inlet} = \frac{\eta}{K} \left\{ \frac{1}{2.55} u_e^2 + \frac{51}{48} u_s^2 \right\}. \tag{4}$$

Figure 8 a and b shows  $\overline{\Delta T}_{inlet}$  as a function of  $u_e$ , assuming that the thermal conductivity of the PAG aqueous solutions can be estimated from the values for water (0.602 W/m·K) and ethylene glycol (0.250 W/m·K), respectively. Within the hypothesis of this model,  $\overline{\Delta T}_{inlet}$  does not exceed 1 °C for any PAG aqueous solutions over the whole range of the entrainment speeds used in the experiment. This estimate confirmed that shear heating does not contribute to gelation in the inlet zone, and the ensuing enhancement of film thickness.

Next, we focused on PAG over-condensation in the inlet region. Hoshi et al. [28] observed that the concentration of polyethylene glycol increased at the inlet of the EHL contact region for water–glycol hydraulic fluids using a micro-FT-IR method. They mentioned that this overconcentration increases the viscosity in the inlet zone. To estimate the

possible increase of the PAG concentration in our experiments, the effective concentration  $c_{eff}$  was defined from the effective viscosity and the relation between the plateau viscosity and the PAG concentration. Figure 9a shows the plateau viscosity as a function of the PAG concentration: it can be seen as a calibration curve. This experimental relation was used in Fig. 9b to estimate an effective PAG concentration in the inlet and to plot its evolution with the entrainment speed. At an entrainment speed of 0.8 m/s, the apparent concentration of the 10 and the 20% PAG aqueous solutions increases to approximately 24 and 30%, respectively. These differences are much more significant than those observed by Hoshi et al. [28]. In addition, the maximum effective concentration of the 10 and the 20% aqueous solutions reached approximately 36 and 42%, respectively, at which point the solutions form a gel. Thus, there could be even more possible factors that enhanced the effective concentration.

Finally, we suggested above that the formation of boundary layers of PAG molecules would also increase the effective viscosity. Guangteng and Spikes [29] proposed that viscous boundary layers with a thickness of 1–10 nm enhanced the film thickness compared to the prediction of Hamrock–Dowson. As discussed above, the effective

**Fig. 8** Estimate of the inlet temperature rise calculated by Eq. (4) [27] with the thermal conductivity of that of **a** water and **b** ethylene glycol, respectively

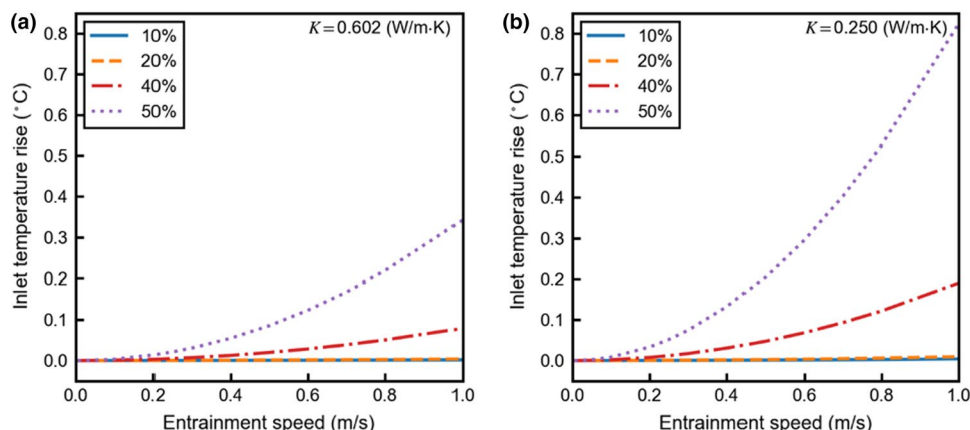
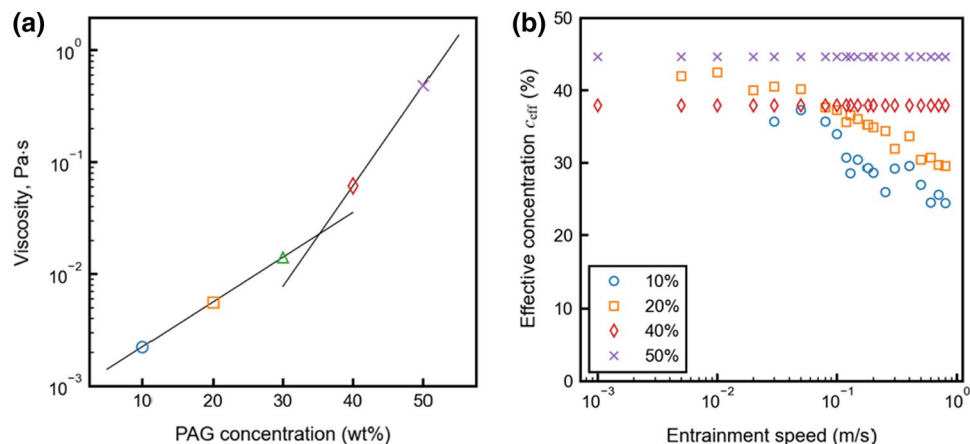


**Fig. 9 a** Viscosity variation as a function of the PAG concentration at 22 °C. The solid lines are linear regression of the viscosity vs. the PAG concentration. **b** Effective concentration,  $c_{eff}$ , as a function of the entrainment speed.  $c_{eff}$  was calculated using the relation obtained in (a)



concentration was estimated to be much higher than the bulk concentration, which can be supported by the boundary effect. Additional careful observations of the static contact, after the experiments, confirm the adsorption of polymer on the surface in the form of patches (see supplemental information).

Regarding the gels in Fig. 9 b, the effective concentration remained roughly constant, and lower than their bulk concentration (if further shear-thinning occurs, the effective concentration could reach the bulk one), indicating that water molecules may preferably go through the sheared network formed by the PAG molecules in the contact area.

## 5 Conclusions

The film-forming capability of PAG aqueous solutions with different concentrations involving sol/gel transition in the EHL regime was analyzed using a combination of rheological measurements, in-situ film thickness measurements, and the framework of Moes–Venner’s formula.

This approach allows the creation of a film formation map where all the aqueous solution data collapsed onto the “isoviscous limit” of the film thickness evolution with the entrainment product, demonstrating that PAG aqueous solutions could be considered as isoviscous. Conversely, pure PAG was considered as a piezoviscous fluid.

For the isoviscous solutions, two families were subsequently defined from the behavior in the contact inlet zone, consistent with the gelation temperature determination and observation of the appearance of a gel. High concentration solutions behaved as gels, forming thinner films than expected. On the contrary, low concentration solutions resulted in a sol. These liquids formed thicker films than expected: this was discussed and attributed to an effective viscosity in the inlet zone, which varies with the velocity, as a result of an effective concentration change.

**Supplementary Information** The online version contains supplementary material available at <https://doi.org/10.1007/s11249-022-01640-0>.

**Authors Contributions** All authors have contributed equally to this work.

**Data Availability** Supporting information is available from the corresponding author, JCB, upon reasonable request.

## Declarations

**Conflict of interest** The authors have no conflicts of interest to declare.

**Open Access** This article is licensed under a Creative Commons Attribution 4.0 International License, which permits use, sharing, adaptation, distribution and reproduction in any medium or format, as long as you give appropriate credit to the original author(s) and the source, provide a link to the Creative Commons licence, and indicate if changes were made. The images or other third party material in this article are included in the article's Creative Commons licence, unless indicated otherwise in a credit line to the material. If material is not included in the article's Creative Commons licence and your intended use is not permitted by statutory regulation or exceeds the permitted use, you will need to obtain permission directly from the copyright holder. To view a copy of this licence, visit <http://creativecommons.org/licenses/by/4.0/>.

## References

- Mohrenstein-Ertel, A. (1984) Die Berechnung tierhydro-dynamischen Schmierungs gekrümmter oberflächen unter hoher Belastung und Relativbewegung. Fortschr. Bet. VDIZ., Reihe 1, No 115, Dsseldorf, ISBN3–18–141501–4
- Hamrock, B.J., Dowson, D.: Isothermal elastohydrodynamic lubrication of point contacts: part 1—theoretical formulation. *J Lubr Technol.* **98**, 223–228 (1976). <https://doi.org/10.1115/1.3452801>
- Moes, H.: *Lubrication and Beyond*. Twente University Press, Enschede (2000)
- Boure, Ph. (1999) *Lubrification et usure du contact fil/outil en treillage humide*. PhD thesis, n°99–47, Ecole Centrale de Lyon
- Raviv, U., Klein, J.: Fluidity of bound hydration layers. *Science* **297**, 1540–1543 (2002). <https://doi.org/10.1126/science.1074481>
- Raviv, U., Giasson, S., Kampf, N., Gohy, J.-F., Jérôme, R., Klein, J.: Lubrication by charged polymers. *Nature* **425**, 163–165 (2003). <https://doi.org/10.1038/nature01970>
- Lee, S., Müller, M., Heeb, R., Zürcher, S., Tosatti, S., Heinrich, M., Amstad, F., Pechmann, S., Spencer, N.D.: Self-healing behavior of a polyelectrolyte-based lubricant additive for aqueous lubrication of oxide materials. *Tribol Lett.* **24**, 217 (2006). <https://doi.org/10.1007/s11249-006-9121-9>
- Giasson, S., Spencer, N.D.: *Aqueous Lubrication with Polymer Brushes*. In: Spencer, N.D. (ed.) *Aqueous Lubrication: Natural and Biomimetic Approaches*. World Scientific Publishing Co Pte Ltd., Singapore (2014)
- Bouré, Ph., Mazuyer, D., Georges, J.-M., Lubrecht, A.A., Lorentz, G.: Formation of boundary lubricating layers with water-based lubricant in a concentrated elastohydrodynamic contact. *J Tribol.* **124**, 91–102 (2002). <https://doi.org/10.1115/1.1398549>
- Fay, H., Cayer-Barrioz, J., Mazuyer, D., Mondain-Monval, O., Ponsinet, V., Meeker, S.: Lubrication mechanisms of lamellar fatty acid fluids. *Tribol Lett.* **46**, 285–297 (2012). <https://doi.org/10.1007/s11249-012-9951-6>
- Spikes, H.A.: Wear and fatigue problems in connection with water-based hydraulic fluids. *J Synthetic Lubr.* **4**, 115–135 (1987). <https://doi.org/10.1002/jsl.3000040203>
- Kimura, Y., Okada, K.: Film thickness at elastohydrodynamic junctions lubricated with oil-in-water emulsions. *Proc. I. Mech. Eng.* **176**, 85–90 (1987)
- Zhu, D., Biresaw, G., Clark, S.J., Kasun, T.J.: Elastohydrodynamic lubrication with O/W emulsions. *J Tribol.* **116**, 310–319 (1994). <https://doi.org/10.1115/1.2927216>
- Wan, G.T.Y., Kenny, P., Spikes, H.A.: Elastohydrodynamic properties of water-based fire-resistant hydraulic fluids. *Tribol Int.* **17**, 309–315 (1984). [https://doi.org/10.1016/0301-679x\(84\)90093-8](https://doi.org/10.1016/0301-679x(84)90093-8)
- Nakahara, T., Makino, T., Kyogoku, K.: Observations of liquid droplet behavior and oil film formation in O/W type emulsion

- lubrication. *J Tribol.* **110**, 348–353 (1988). <https://doi.org/10.1115/1.3261630>
16. Kimura, Y., Okada, K.: Lubricating properties of oil-in-water emulsions. *Tribol T.* **32**, 524–532 (1989). <https://doi.org/10.1080/10402008908981921>
  17. Nakahara, T., Shiokawa, S., Kyogoku, K.: Phase inversion region in O/W emulsion lubrication. *J. of Jap. Soc. of Tribologists.* **35**, 1435–1446 (1990)
  18. Barker, D.C., Johnston, G.J., Spikes, H.A., Bünemann, T.F.: EHD film formation and starvation of oil-in-water emulsions. *Tribol T.* **36**, 565–572 (1993). <https://doi.org/10.1080/10402009308983196>
  19. Bonyadi, S.Z., Hasan, M.M., Kim, J., Mahmood, S., Schulze, K.D., Dunn, A.C.: Review: friction and lubrication with high water content crosslinked hydrogels. *Tribol Lett.* **68**, 119 (2020). <https://doi.org/10.1007/s11249-020-01352-3>
  20. Matlock, P., Brown, W., Clinton, N.: Synthetic lubricants and high- performance functional fluids revised and expanded. *Chem Indust.* **19990720**, 159–193 (1999). <https://doi.org/10.1201/9780203909898.ch6>
  21. Mueller, E. R., Martin, W.H.: Poly-alkylene glycol lubricants: uniquely water soluble. *Lubr Eng.* **31**(7), 348–356 (1975).
  22. Zhang, C.H., Zhao, Y.C., Björling, M., Wang, Y., Luo, J.B., Prakash, B.: EHL properties of polyalkylene glycols and their aqueous solutions. *Tribol Lett.* **45**, 379–385 (2012). <https://doi.org/10.1007/s11249-011-9883-6>
  23. Liu, S., Guo, D., Xie, G.: Nanoscale lubricating film formation by linear polymer in aqueous solution. *J Appl Phys.* **112**, 104309 (2012). <https://doi.org/10.1063/1.4765674>
  24. Ernesto, A., Mazuyer, D., Cayer-Barrioz, J.: The combined role of soot aggregation and surface effect on the friction of a lubricated contact. *Tribol Lett.* **55**, 329–341 (2014). <https://doi.org/10.1007/s11249-014-0365-5>
  25. de Gennes, P.G.: *Scaling concepts in polymer physics.* Cornell University Press, Newyork (1979)
  26. Vergne, P., Kamel, M., Querry, M.: Behavior of cold-rolling oil-in-water emulsions: a rheological approach. *J Tribol.* **119**, 250–258 (1997). <https://doi.org/10.1115/1.2833173>
  27. Guilbault, R.: A simplified thermal analysis of elastohydrodynamic contacts. *J Tribol.* **135**, 021502 (2013). <https://doi.org/10.1115/1.4023085>
  28. Hoshi, Y., Minami, I., Mori, S.: Change in concentration of water-glycol hydraulic fluid near EHL contact region: observation by micro FT-IR. *Japanese Journal of Tribology.* **49**, 599–610 (2004)
  29. Guangteng, G., Spikes, H.A.: Boundary film formation by lubricant base fluids. *Tribol Trans.* **39**, 448–454 (1996). <https://doi.org/10.1080/10402009608983551>

**Publisher's Note** Springer Nature remains neutral with regard to jurisdictional claims in published maps and institutional affiliations.